Computational Materials Science 101 (2015) 96–107

Contents lists available at ScienceDirect

Computational Materials Science

journal homepage: www.elsevier.com/locate/commatsci

Vacancy formation energies in metals: A comparison of MetaGGA with LDA and GGA exchange–correlation functionals

Bharat Medasani [a,*], Maciej Haranczyk [a], Andrew Canning [a,d], Mark Asta [b,c,d,1]

[a] Computational Research Division, Lawrence Berkeley National Laboratory, Berkeley, CA 94720, United States
[b] Department of Materials Science & Engineering, University of California, Berkeley, CA 94720, United States
[c] Material Sciences Division, Lawrence Berkeley National Laboratory, Berkeley, CA 94720, United States
[d] Department of Chemical Engineering & Materials Science, University of California, Davis, CA 95616, United States

ARTICLE INFO

Article history:
Received 22 September 2014
Received in revised form 13 January 2015
Accepted 16 January 2015
Available online 9 February 2015

Keywords:
Metals
Vacancy formation energy
MetaGGA

ABSTRACT

We report on the results of density-functional-theory based calculations of the vacancy formation energies in metals using the revised Tao–Perdew–Staroverov–Scuseria (revTPSS) functional (Pedrew et al., 2009), which is a self-consistent semilocal meta-generalized gradient approximation functional. The motivation for this work is to determine if the improved accuracy of surface energies for revTPSS compared to local and generalized gradient approximation functionals also leads to improved vacancy formation energies since vacancies can be viewed as internal surfaces. In addition, we report on the lattice constants, cohesive energies and bulk moduli predicted by revTPSS. By comparing the vacancy formation energies and bulk properties, the performance of revTPSS is assessed against four functionals: the local spin density approximation (LSDA), Perdew, Burke and Ernzerhof (PBE), Perdew–Wang-91 (PW91), and PBE for solids (PBEsol). Using an automated computational approach, we calculate the vacancy formation energies and the macroscopic properties of 34 metal systems for the five functionals. For macroscopic properties (lattice constants, cohesive energies and bulk modulus), we find the results for revTPSS typically lie between LDA and PBE with a mean absolute percentage deviation of 1.1% and 12.1% from the experimental data for lattice constants and cohesive energies respectively. Further, it is found that revTPSS predicts higher vacancy formation energies when compared to the four other functionals surveyed. We have observed the following order for the functionals with respect to the computed vacancy formation energies, $E_f^{xc}: E_f^{revTPSS} > E_f^{PBEsol} \sim E_f^{LDA} > E_f^{PBE} > E_f^{PW91}$. We also consider the effects of a surface-energy error correction that has been proposed for standard LDA and GGA functionals. This correction increases the vacancy formation energies of LDA, PBE and PW91 functionals. The revTPSS computed VFEs are greater than the surface-energy-corrected PBE VFEs by a mean relative difference of 14.8%.

1. Introduction

Understanding defects in crystalline solids is essential for characterizing their thermal, electrical and mechanical behavior. Vacancies are known to be the dominant equilibrium point defects in elemental metals and many close-packed intermetallic compounds. An intrinsic property of these point defects is the vacancy formation energy (VFE) E_f, which is a major factor in determining the equilibrium concentration at finite temperature [1–3].

Experimentally, VFE in metals is indirectly determined from the vacancy concentration, which is derived from measurements of quantities such as positron lifetimes in positron annihilation spectroscopy (PAS), specific heat measurements in calorimetric methods, lattice expansion in differential dilatometry (DD), and electrical conductivity measurements in resistivity experiments. Despite extensive efforts over the last few decades, experimental data on VFEs for some metals and for many intermetallic compounds is not yet available [4,5]. Additionally, a wide scatter in the values for VFEs is often reported by different experimental methods [5].

In deriving the VFEs from the vacancy concentrations measured at different temperatures in PAS and DD, it is common to use the formula, $c_v = exp[-(H_F - TS_F)/k_BT]$, assuming that the formation enthalpy (H_F) and entropy (S_F) are constants, independent of temperature, as they would be in a harmonic crystal. With these assumptions, the vacancy formation enthalpy can be derived from the slope of an Arrhenius plot of the logarithm of c_v versus $1/T$.

* Corresponding author.
E-mail addresses: mbkumar@gmail.com (B. Medasani), mdasta@berkeley.edu (M. Asta).
[1] Principal corresponding author.

http://dx.doi.org/10.1016/j.commatsci.2015.01.018
0927-0256/

However, in a recent article [6], Glensk et al. have demonstrated that the consideration of anharmonic contributions to the vibrational free energy can lead to sizeable corrections in the values of VFEs derived from such an analysis. Specifically, Glensk et al. showed that anharmonic contributions result in a correction to the VFE of −0.17 eV for Cu, which is 17% of the magnitude of this quantity. For Al, the correction was smaller, at −0.01 eV (1.5%).

Kraftmakher, by assuming a linear temperature dependent formation entropy, computed formation enthalpies from specific heat measurements. The 0 K formation enthalpies reported from specific heat data for Al and Cu are 0.71 eV and 0.86 eV respectively [4]. However, these differ from the local Grüneisen theory (LGT) corrected PAS + DD VFEs reported by Glensk et al., which are 0.66 eV and 1.06 eV respectively [6]. The discrepancies between the analyses is an example of the difficulties inherent in extracting VFEs from the experimental data in metals.

The advent of Kohn–Sham density functional theory (DFT) has greatly advanced accurate theoretical predictions of materials properties [7–9]. The increasing availability of computational power has enabled rapid growth in the number of materials and the properties that can be studied. The accuracy of the DFT approach depends crucially on the nature of the approximation used for the exchange correlation (XC) functional. Often, the generalized gradient approximation (GGA) [10–12], which incorporates electron density and the gradient of electron density in the XC functional, performs better than the simpler local spin density approximation (LDA) [7,13], which incorporates only local electron spin densities. Among many GGA functionals available, the functionals developed by Perdew, Burke and Ernzerhof [10] and by Perdew and Wang [11,12], commonly referred to as PBE and PW91 respectively, are widely used.

Within the last two decades, many first principles theoretical studies on VFEs in metals have been published [14–23,6,24]. The difference between the vacancy formation energies (VFEs) given by LDA and PBE for metals is often significant. For example, PBE VFEs for silver, gold, iridium, and platinum are lower by 24%, 32%, 20%, and 27% respectively when compared with the LDA VFEs [23]. In a few cases, even the standard GGA functionals, PBE and PW91, which are often used interchangeably due to their almost identical performance for lattice constants and cohesive energies, predict quite different values for the vacancy formation energies [25]. For example, in the case of aluminum, the difference is 18% [23]. Also, LDA VFEs are often in better agreement with the reported experimental values [15,23].

The differences between GGA and LDA functionals with respect to vacancy formation energies of metals is similar to that of the surface energies of the respective metals [26,27]. In addition, the electron density profile at the edge of the vacancy is similar to the electron density profile at the metal surface. These similarities led to the concept of a "surface energy error correction" to improve the performance of GGA functionals in predicting VFEs in metals. The known error in DFT computed unit surface energy is utilized in improving the computed vacancy formation energy [18,19,28,21,29,23].

Broadly classified, there are two approaches to surface energy error correction. In the first approach, to reduce the surface energy errors in the VFEs computed with the standard GGA functionals, an *a posteriori* correction is applied. Carling et al. applied the *a posteriori* correction to reduce the discrepancy between the DFT computed and the experimental VFE for aluminum [18]. By scaling the surface area of the vacancy in Al with the lattice parameter as a scaling constant, Mattsson and Mattsson computed the correction for Pt, Pd and Mo [19]. Using a similar approach, Nandi et al. evaluated the correction for Ni, Fe and Cr [21]. Nazarov, Hickel and Neugebauer calculated the correction for twelve fcc metals by minimizing the difference between the surface energy error corrected VFEs of LDA, PBE and PW91 functionals [23].

In the second approach, to improve upon the VFEs computed within the generalized gradient approximation, newer GGA functionals incorporating surface energy error correction, such as PBE for solids (PBEsol) [30], local airy gas (LAG) [31] and Armiento–Mattson-05 (AM05) [28] have been proposed by Perdew et al., Vitos et al., and Armiento and Mattson respectively. Of these newer functionals, AM05 and PBEsol, though developed from different principles give almost identical values for lattice constants and bulk moduli [32]. The VFEs predicted by AM05 have been reported for twelve fcc metals [23], and the PBEsol VFEs are available for three fcc metals: Al, Ni and Cu [17,16].

Both the surface energy error correction approaches increase the GGA computed VFEs and bring them closer to the LDA value and hence to the experimentally reported VFEs. However, LGT corrected PAS + DD VFEs for Al and Cu reported by Glensk et al. have a better agreement with GGA VFEs.

In the last decade, many newer functionals, classified under meta-GGA, have been proposed [33–36]. These functionals incorporate either the Laplacian of the electron density or the electron kinetic energy density or both, in addition to the density and the density gradient. The kinetic energy density operators are utilized in systematically improving the exchange energy predicted by the functionals by recovering the higher orders in the Taylor expansion of the exchange energy when compared with GGA functionals [34,37]. As a result meta-GGA functionals predict good atomization and surface energies [34,38] and are expected to have better accuracy in predicting the VFEs due to the improved semilocal approximation [16]. These functionals have only recently been implemented in the popular density functional codes. So far, to our knowledge, no vacancy formation energies predicted with these functionals have been reported. Due to the simultaneous presence of rapid and slow electron density variations in the vacancy structures, vacancy formation energy serves as an interesting benchmark to evaluate the accuracy of the newer meta-GGA functionals.

In the current work, we report on the performance of a meta-GGA functional in predicting the vacancy formation energies in metals. For this purpose, we choose revised Tao–Perdew–Staroverov–Scuseria (revTPSS), which is a self consistent meta-GGA functional [34,35,38]. In the construction of the revTPSS functional, second-order gradient expansion for exchange is recovered over a wide range of densities. In addition, revTPSS minimizes the overprediction of correlation energy of surfaces when compared to PBE. It also has the advantage of being only about 30% slower than PBE [38]. We report the VFEs computed with revTPSS for a broad range of metals. For comparison purposes, we have surveyed four additional functionals: LDA, PBE, PW91, PBEsol. For the VFEs computed with LDA, PBE and PW91 functionals, we also applied surface energy error corrections. Of the available schemes for the correction, we choose the one proposed by Nazarov et al. [23] due to its suitability for high throughput computing. The resulting surface error corrected VFEs are compared with the revTPSS computed VFEs. In this work, for all the elements, we use the crystal structure of the allotrope that is observed experimentally at room temperature. For a few elements such as Os, Co, and Tc, multiple allotropes are considered.

The remainder of the paper is organized as follows. The next section describes the computing methodology and the theory behind surface energy error correction schemes. In the following results section, we discuss the bulk properties such as cohesive energies and lattice constants computed with the five functionals. Then we discuss the vacancy formation energies and analyze the correlation between the macroscopic properties and the vacancy formation energies.

2. Methodology

2.1. Computational details

We used the Vienna *ab initio* simulation package (VASP) [39–41] to perform DFT calculations. All the DFT calculations were automated using a modified version of the high throughput framework of the Materials Project [42] and the related pymatgen toolset [43]. We used the projector augmented wave (PAW) formalism based potentials for the five exchange correlation functionals studied [44,45]. For PBEsol and revTPSS functionals, PBE based PAW potentials were used. For all the calculations a cut-off value of 520 eV was used for the plane-wave basis set. Spin polarization was used in all the calculations. For electronic smearing, the first-order Methfessel Paxton method [46] with a smearing width of 0.2 eV was used. For all magnetic elements, only the ferromagnetic state is considered. For Cr, however, this differs from the magnetic ground state, where different calculations yield either an anti-ferromagnetic state or a spin-density wave [47].

The supercell approach was used in the computation of vacancy formation energies. In this approach, the vacancy formation energy, E_f, is given by

$$E_f = E_{tot}^{vac} - \frac{N-1}{N} E_{tot}^{blk}, \tag{1}$$

where E_{tot}^{vac} is the total energy of the vacancy supercell, E_{tot}^{blk} is the total energy of the bulk supercell and N is the number of atoms in the bulk supercell. The bulk supercell was generated from the optimized primitive cell and the vacancy supercell was generated by removing an atom from the bulk supercell. The atomic positions in the vacancy supercell were then relaxed at constant volume.

The primitive cell, which was the starting point in the calculation of VFEs, was optimized by relaxing the volume and atomic positions at fixed geometry. For primitive cell relaxation, we used a $25 \times 25 \times 25$ Gamma centered k-point grid. At these settings, the lattice constants were converged to within 0.01% for fcc Al, 0.6% for bcc K, and 0.3% for hcp Re.

The vacancy supercell was optimized by relaxing the atomic positions at constant volume until the total energy of the structure was converged to within 1 meV. After testing for convergence of VFE with respect to supercell size, we used a $2 \times 2 \times 2$ supercell (32 atoms) for fcc structures, a $4 \times 4 \times 4$ supercell (128 atoms) for bcc structures and a $3 \times 3 \times 2$ supercell (36 atoms) for hcp structures. Supercell sizes equal to these were reported to be sufficient for calculating the VFEs in metals, provided the Brioullion zone was sufficiently sampled [14,15,17,23,24]. After testing for convergence, we found that Monkhorst–Pack k-point grid of size $4 \times 4 \times 4$ and Gamma centered grids of size $11 \times 11 \times 11$ and $11 \times 11 \times 11$ are sufficient for bccc, fcc and hcp structures respectively at the supercell sizes used. With respect to k-points, plane wave basis set size and supercell sizes, the convergence tests on fcc Al, bcc V and hcp Re showed that the vacancy formation energies were converged to within 0.01 eV, 0.02 eV, and 0.01 eV respectively. The plane wave cutoff and k-point grid size were kept constant for both vacancy and bulk supercell total energy calculations.

2.2. Posteriori surface error correction

It has been posited that the rapid variation in the charge density at the edge of the vacancy resembles an internal surface within the structure and this surface gives rise to an error in the computed vacancy formation energy for Eq. (1). Many correction schemes have been proposed to mitigate this error [18,19,23,21]. The origin of these surface error correction schemes lies in making use of the known errors in surface energies of jellium surface models given by different XC functionals. The error in surface energy for unit surface area in the jellium model, $\Delta\sigma_{xc}$, was parameterized by Mattsson et al. [48] in the form,

$$\Delta\sigma_{xc}(\tilde{r}_s) = A_{xc}\tilde{r}_s^{-5/2} + B_{xc}\tilde{r}_s^{-3/2}, \tag{2}$$

where $\tilde{r}_s$ is the normalized radius of sphere of a single electron. $\tilde{r}_s$ is, in turn, dependent on electron density and is defined as

$$\tilde{r}_s = \frac{[3/(4\pi\bar{n})]^{-1/3}}{a_0} \tag{3}$$

where $\bar{n}$ is the average electron density and a_0 is the Bohr radius. The values of A_{xc} and B_{xc} for LDA, PBE, and PW91 are given in Table 1.

To compute the total surface energy error, in addition to knowing the error per unit area, knowledge of the surface area of the vacancy is also needed. Of the different schemes available to compute the vacancy surface area, the scheme introduced by Nazarov et al. [23] lends itself well to a high throughput approach because all the inputs for the correction scheme can be computed dynamically. The surface correction obtained from this approach is close to that obtained from the method proposed by Mattsson et al. [48]. In this scheme, the surface area of a vacancy is considered unknown. However, an approximation is made that the reduced surface area, which is surface area scaled down by the square of the lattice parameter, is equal for all functionals, LDA, PBE and PW91. The surface error corrected vacancy formation energy, $\widetilde{E}_{xc}^{f}$, is then given by

$$\widetilde{E}_{xc}^{f} = E_{xc}^{f} + x(a_{xc})^2 \Delta\sigma_{xc}^{cor}(\tilde{r}_s), \tag{4}$$

where E_{xc}^{f} and a_{xc} are the uncorrected VFE and the lattice constant respectively, and x is the reduced surface area that needs to be determined. We have three equations corresponding to LDA, PBE and PW91 and two unknowns, x and $\widetilde{E}_{xc}^{f}$. The best values for x and $\widetilde{E}_{xc}^{f}$ are obtained by using a least squares fit to minimize $\sum_{ij}\Delta_{ij}\widetilde{E}_{xc}^{f} = \sum_{ij}|\widetilde{E}_{xc,i}^{f} - \widetilde{E}_{xc,j}^{f}|^2$ [23].

2.3. Bulk modulus and cohesive energy

To understand the performance of the revTPSS functional in predicting macroscopic properties, bulk modulus and cohesive energies were computed. To calculate the bulk modulus, B_0, the volume of the optimized unit cell was varied from 91% to 109% and energies were calculated at 15 different points. B_0 was obtained by fitting the 15 energy-volume points to the third order Birch–Murnaghan equation of state [49].

Cohesive energy is defined as the difference between the energy of a free atom to that of bulk atom. The free atom energy was calculated using a symmetry breaking $12 \times 13 \times 14$ Å^3 unit cell and Gamma centered k-point as suggested in the VASP user manual.

3. Results and discussion

Before analyzing the VFEs for metals and the performance of the functionals in calculating the VFEs, we looked at the performance of the functionals in computing the bulk properties of the metals.

Table 1
Unit surface energies of jellium planar surface for different functionals [48].

	LDA	PBE	PW91
A_{xc} (erg/cm^2)	448.454	1193.7	1577.2
B_{xc} (erg/cm^2)	−55.845	−174.37	231.29

This can help in determining whether the deviations in the theoretical VFEs are related to any such deviations in the computed bulk properties. To this end, we computed lattice constants, cohesive energies and bulk moduli and the calculated data is compiled in Table 2–10.

Table 2–4 show that LDA, PBEsol and revTPSS underpredict the lattice constants, whereas PBE and PW91 overpredict the lattice constants. The revTPSS computed lattice constants, on average, differ from the experimental data compiled in Ref. [50] by 1.1%. This is equal to the accuracy of PBE, and better than that of LDA, PW91 and PBEsol whose lattice constants on average differ from the experimental values by 2.8%, 1.2% and 1.4% respectively. The maximum deviation is observed for Cr, V, and Na, where revTPSS underestimates the lattice constants by 3.3%, 2.6% and 2.2% respectively. On the other hand, for Rb, revTPSS overestimates by 2.1%. The lattice constants of bcc structures computed with the PBE functional are in good agreement with the PBE data published by Wang et al. [51] with an average difference of 0.3%. Similarly, our PBE lattice constants of fcc structures differ from the data published by Angsten et al. by 0.9%.

Fig. 1 shows the correlation between the experimental data and the cohesive energies calculated with various functionals. The experimental data is taken from the values compiled in Ref. [52]. The correlation coefficient or *r*-value is either 0.98 or 0.99 for all the functionals indicating that the theoretical values are highly correlated with the experimental data. The plot for LDA shows that it consistently overestimates the cohesive energy for all the metals. The red line shows the correlation between the experimental and LDA cohesive energies and it has a slope of 1.25 indicating that the LDA results deviate more from the experimental values when the cohesive energy values are higher. For alkali metals, the cohesive energies predicted by LDA agree with the experimental values to within 13%. However there is a significant discrepancy between the theoretical and experimental data for elements with higher cohesive energies. This results in a mean absolute percentage deviation (MAPD) of 30.5% between LDA and experimental cohesive energies. The results for PBE, on the other hand, have a better match with the experimental data with the MAPD being only 11.6%. The PBE cohesive energy plot shows that PBE under-estimates cohesive energies for metals with small cohesive energy values and over-estimates for metals with higher cohesive energies. The correlation line for PBE has a slope of 1.05 and crosses over from the under-predicted region to the over-predicted region as the cohesive energies increase. Both PBEsol and revTPSS exhibit nearly identical behavior and their linear correlation lines have slopes of 1.11 and 1.10 respectively. Interestingly these slopes are intermediate between the LDA and PBE linear correlation slope values. For bcc metals, PBEsol estimates cohesive energies matching the experimental values at all ranges except for Fe, Cr and Ta. For metals of other crystalline structures, both PBEsol and revTPSS over-predict when compared to experiment. The MAPD with experimental data for PBEsol and revTPSS are 16.8% and 12.1% respectively. The revTPSS cohesive energy for Ti is missing from the tables as we had problems with convergence. A few of the later results for bulk moduli are also missing for the same reason. Using our high throughput automated approach results that do not converge are automatically flagged and not included in the database although we did restart many of them with different choices for the algorithms to try and gain convergence.

Fig. 2 shows the correlation between the experimental bulk moduli given in Ref. [53,54] and the theoretical bulk moduli of metals computed with different functionals. The plots have correlation coefficients in the range of 0.93–0.95, which is less than the correlation coefficient of cohesive energy plots. Significant deviation between the experimental and the theoretical values in the case of elements like Cr, Ru, Rh, and Os contributes to the reduction of the correlation coefficient. From the plots, it is clear that the performance of the functionals in predicting bulk moduli is similar to the performance in predicting cohesive energy except for some change in the slopes of correlation lines.

The computed VFEs are tabulated in Table 11–13. We could not obtain reliable results for the cases of LDA vanadium and revTVPSS tungsten. The VFEs for LDA and GGA functionals are in good agreement with the data reported by Angsten et al. [24] and Nazarov et al. [23]. Fig. 3 and 4 show the comparison between the vacancy formation energies computed with different functionals and the corresponding experimental data where available. In Fig. 3, for experimental values, positron annihilation spectroscopy (PAS) data compiled in Landolt–Bornstein database is used. In PAS experiments, vacancy concentrations are measured from either the positron lifetimes or Doppler broadening or the angular correlation of γ-quanta assuming a temperature independent vacancy formation enthalpy and entropy. Glensk et al. using finite temperature first principles DFT recently reported that anharmonic contributions to the vacancy formation free energy lead to a correction to the VFE extrapolated from high temperature of 0.18 eV for Cu and 0.01 eV for Al. This makes the comparison of PAS experimental VFEs with DFT computed VFEs subject to uncertainties.

The plots in Fig. 3 indicate that the VFEs are clustered based on the crystalline structure symmetry and the element positions in the periodic table. Overall for fcc metals, the revTPSS VFEs are the closest to the experimental values. LDA, PBE and PBEsol under-predict the VFE for fcc metals when compared with the experimental values while revTPSS overestimates for Ag, Al, Cu and Ni. Applying the LGT correction [6], the difference between the experimental and revTPSS VFEs further increases to 0.44 eV for Cu, which is at 41.5% MAPD. For LDA, PBE and PBEsol functionals, the difference between the experimental and theoretical values is greater for the 2nd and 3rd row transition metals such as Au, Pt, Pd and Rh when compared with the other elements. For all bcc

Table 2
Lattice constant (in Å) predicted by different functionals for fcc metals.

Element	LDA	PBE	PW91	PBEsol	revTPSS	Experiment [50]
Ag	4.00	4.15	4.16	4.05	4.06	4.09
Al	3.98	4.04	4.05	4.02	4.01	4.05
Au	4.05	4.16	4.17	4.08	4.08	4.08
Ca	5.37	5.56	5.51	5.46	5.51	5.59
Co	3.42	3.52	3.52	3.46	3.47	–
Cu	3.52	3.63	3.64	3.57	3.56	3.61
Ir	3.82	3.87	3.88	3.83	3.83	3.84
Ni	3.42	3.52	3.52	3.46	3.46	3.52
Os	3.81	3.86	3.86	3.82	3.82	–
Pb	4.88	5.04	5.04	4.93	4.95	4.95
Pd	3.84	3.94	3.96	3.87	3.88	3.89
Pt	3.90	3.97	3.99	3.92	3.92	3.92
Rh	3.75	3.82	3.84	3.77	3.78	3.80
Tc	3.80	3.86	3.88	3.82	3.83	–

Table 3
Lattice constant (in Å) predicted by different functionals for bcc metals.

Element	LDA	PBE	PW91	PBEsol	revTPSS	Experiment [50]
Cr	2.79	2.84	2.85	2.81	2.82	2.91
Fe	2.75	2.83	2.83	2.79	2.80	2.87
K	5.05	5.28	5.28	5.21	5.34	5.33
Mo	3.11	3.15	3.15	3.12	3.13	3.15
Na	4.05	4.19	4.19	4.18	4.19	4.29
Nb	3.26	3.32	3.32	3.29	3.30	3.30
Ta	3.25	3.31	3.31	3.27	3.27	3.30
Ti	3.16	3.25	3.25	3.21	3.21	–
V	2.91	2.98	2.98	2.94	2.95	3.03
W	3.13	3.17	3.18	3.14	3.14	3.17

Table 4
Lattice constant (in Å) predicted by different functionals for hcp metals.

Element	LDA		PBE		PW91		PBEsol		revTPSS		Experiment [50]	
	a	c	a	c	a	c	a	c	a	c	a	c
Co	2.43	3.91	2.49	4.03	2.49	4.03	2.45	3.96	2.46	3.98	2.51	4.07
Hf	3.12	4.93	3.19	5.04	3.20	5.05	3.15	4.98	3.15	4.98	3.20	5.05
Mg	3.12	5.08	3.19	5.19	3.19	5.19	3.16	5.14	3.18	5.17	3.21	5.21
Os	2.72	4.29	2.75	4.34	2.76	4.35	2.73	4.31	2.73	4.31	2.73	4.32
Re	2.74	4.42	2.77	4.48	2.78	4.48	2.75	4.44	2.77	4.50	2.76	4.46
Ru	2.67	4.22	2.71	4.28	2.73	4.30	2.69	4.24	2.69	4.25	2.71	4.28
Sc	3.23	4.98	3.32	5.16	3.31	5.14	3.28	5.08	3.28	5.11	3.31	5.27
Tc	2.70	4.32	2.74	4.39	2.76	4.41	2.72	4.34	2.72	4.35	2.74	4.39
Ti	2.86	4.54	2.94	4.65	2.93	4.64	2.90	4.59	2.89	4.58	2.95	4.69
Tl	3.42	5.41	3.59	5.61	3.59	5.60	3.47	5.48	3.47	5.51	3.46	5.52
Y	3.54	5.51	3.65	5.67	3.65	5.66	3.60	5.58	3.57	5.51	3.65	5.73
Zn	2.58	4.72	2.66	4.94	2.64	5.09	2.62	4.78	2.60	4.61	2.66	4.95

Table 5
Cohesive energies (in eV) of fcc metals computed with different functionals.

Element	LDA	PBE	PW91	PBEsol	revTPSS	Experiment [52]
Ag	3.61	2.52	2.53	3.06	3.04	2.95
Al	4.01	3.43	3.41	3.81	3.44	3.39
Au	4.29	3.04	3.03	3.71	3.63	3.81
Ca	2.22	1.91	1.91	2.11	1.65	1.84
Co	6.65	5.12	5.18	5.94	7.31	–
Cu	4.50	3.48	3.47	4.03	4.15	3.439
Ir	9.35	7.29	7.33	8.38	8.17	6.94
Ni	6.06	4.80	4.97	5.86	5.56	4.44
Os	11.21	8.18	8.24	9.42	9.11	–
Pb	3.76	2.94	2.97	3.34	3.20	2.03
Pd	5.06	3.74	3.71	4.47	4.40	3.89
Pt	7.10	5.49	5.57	6.47	6.27	5.84
Rh	7.68	5.72	5.75	6.94	7.23	5.75
Tc	8.75	6.86	6.83	7.82	7.51	–

Table 6
Cohesive energies (in eV) of bcc metals computed with different functionals.

Element	LDA	PBE	PW91	PBEsol	revTPSS	Experiment [52]
Cr	5.54	4.08	4.04	4.72	4.48	4.10
Fe	6.53	4.87	5.20	5.88	5.49	4.28
K	1.01	0.86	0.86	0.92	0.95	0.93
Mo	8.14	6.36	6.33	7.18	6.96	6.82
Na	1.25	1.08	1.09	1.15	1.09	1.11
Nb	8.43	8.52	8.50	7.64	8.27	7.57
Ta	9.64	8.20	8.22	9.27	8.96	8.10
Ti	6.50	5.78	5.17	6.08	5.36	–
V	6.66	5.39	5.34	5.98	5.87	5.31
W	11.81	9.97	8.40	9.27	9.23	8.90

Table 7
Cohesive energies (in eV) of hcp metals and metals with other symmetries.

Element	LDA	PBE	PW91	PBEsol	revTPSS	Experiment [52]
Co	6.63	5.16	5.20	5.96	6.42	4.39
Hf	7.61	6.49	6.50	7.25	7.08	6.44
Os	11.35	8.32	8.37	9.45	9.25	8.17
Re	9.61	7.82	7.83	8.79	8.66	8.03
Ru	8.78	6.78	6.78	7.81	7.53	6.74
Sc	4.93	4.14	4.18	4.73	4.34	3.90
Tc	8.83	6.93	6.90	7.90	7.59	6.85
Ti	6.59	5.77	5.87	6.18	–	4.85
Tl	2.80	2.00	2.05	2.37	2.25	1.88
Y	4.91	4.17	4.22	4.62	4.43	4.37
Zn	1.87	1.09	1.11	1.56	1.74	1.35

Table 8
Bulk modulus (in GPa) for fcc metals.

Element	LDA	PBE	PW91	PBEsol	revTPSs	Experiment
Ag	137	90	91	118	120	100
Al	84	78	74.5	82	84	76
Au	192	139	137	174	176	180
Ca	18.5	17.5	17.5	18	17.8	17
Co	267	208	210	242	243	180
Cu	184	138	138	164	171	140
Ir	404	349	343	389	391	320
Ni	252	196	196	227	236	180
Os	445	397	390	434	439	–
Pb	51.8	39.5	40.4	47	45.8	46
Pd	226	168	167	204	206	180
Pt	306	249	244	289	290	230
Rh	318	257	254	297	297	380
Tc	344	302	300	330	329	–

Table 9
Bulk modulus (in GPa) of bcc metals.

Element	LDA	PBE	PW91	PBEsol	revTPSs	Experiment
Cr	302	259	258	283	292	160
Fe	251	188	188	221	213	170
K	5	3.59	3.54	3.71	3.38	3.1
Mo	302	268	267	290	287	230
Na	9.23	7.81	7.70	7.86	7.57	6.3
Nb	195	173	173	186	187	170
Ta	222	201	200	213	214	200
Ti	122	107	108	114	115	–
V	210	187	187	204	205	160
W	344	313	310	334	337	310

Table 10
Bulk modulus (in GPa) for hcp metals.

Element	LDA	PBE	PW91	PBEsol	revTPSs	Experiment
Co	272	212	213	244	247	–
Hf	125	113	112	120	120	110
Mg	41	37	35	48	38	45
Os	453	405	397	442	447	462
Re	411	372	369	400		370
Ru	370	315	310	352	349	220
Sc	62	54	55	58		57
Tc	346	303	302	332	331	
Ti	1284	113	113	120	116	110
Tl	43	27	28	36	36	43
Y	44	41	42	42		41
Zn	101	73	73	89	91	70

transition metals, revTPSS overestimates the VFEs. For Fe and Cr, all functionals overestimate the VFEs compared to experiment. PBE shows the best agreement with the experimental data for V, Nb and Ta, but underestimates for Mo and W. LDA and PBEsol overestimate for Nb, have good agreement for Ta and Mo and underestimate for W. For bcc alkali metals, there is no significant difference

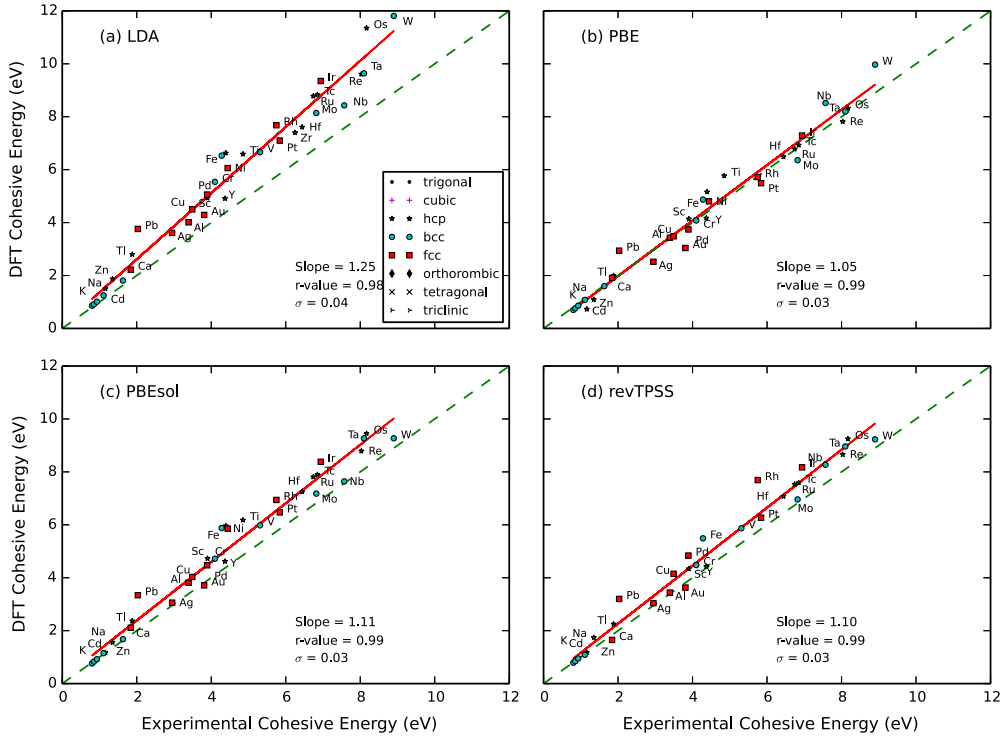

Fig. 1. Comparison between the experimental and theoretical cohesive energies predicted by different functionals. The solid red line represents linear regression of the data and the green dashed line correspond to the case "$x = y$". Here, r-value and σ represent correlation coefficient and error of fit respectively. (For interpretation of the references to color in this figure legend, the reader is referred to the web version of this article.)

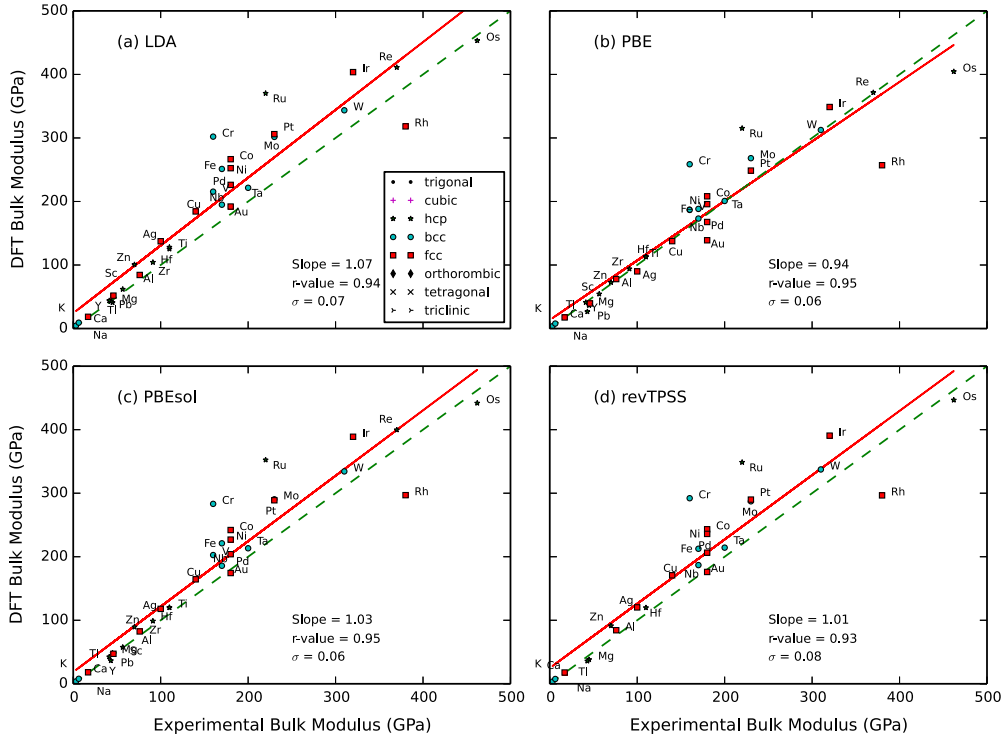

Fig. 2. Comparison between the experimental and the theoretical bulk moduli predicted by different functionals. The definitions of red solid and green dashed lines as well as r-value and σ are given in Fig. 1. (For interpretation of the references to color in this figure legend, the reader is referred to the web version of this article.)

in the performance of the functionals. For hcp Ti and Co, all functionals significantly overpredict the experimental value.

Kraftmakher published vacancy formation energies from specific heat measurements that consider linear temperature dependence of formation entropy [4]. The experimental VFEs reported by Kraftmakher are compared with the DFT values in Fig. 4. There is significant scatter in the data, making it difficult to draw any definitive conclusions. If the 0 K VFE of Cu from specific heat data,

Table 11
Theoretical vacancy formation energies (in eV) predicted by different functionals for fcc metals. E_f and $\widetilde{E}_f$ represent uncorrected and surface energy error corrected formation energies for LDA, PBE and PW91 functionals. Data under SH, ρ, and PAS columns represent specific heat, electrical conductivity and positron annihilation spectroscopy measurements respectively.

El.	LDA		PBE		PW91		PBEsol	revTPSS	Experiment [4,5]		
	E_f	$\widetilde{E}_f$	E_f	$\widetilde{E}_f$	E_f	$\widetilde{E}_f$			SH	ρ	PAS
Ag	1.05	1.09	0.78	0.89	0.77	0.91	0.99	1.25		1.06, 1.11	1.11, 1.31
Al	0.71	0.87	0.65	1.06	0.56	1.09	0.77	0.77	0.66, 0.79 1.17	0.77, 0.8	0.66, 0.68
Au	0.66	0.84	0.41	0.87	0.39	1.01	0.62	0.92	1.0	0.95, 1.02	0.89
Ca	1.23	1.39	1.18	1.54	1.13	1.60	1.22	1.34			
Co	2.10	2.10	1.80	1.80	1.76	1.76	2.03	2.29			
Cu	1.29	1.30	1.09	1.12	1.05	1.08	1.27	1.50	1.05	0.92, 1.0 1.03, 1.3	1.28, 1.42
Ir	1.89	2.05	1.62	2.01	1.57	2.07	1.87	2.22			
Ni	1.68	1.82	1.46	1.82	1.42	1.89	1.65	1.95	1.4	1.4	1.79
Os	3.35	3.40	3.08	3.22	3.02	3.20	3.38	3.71			
Pd	1.48	1.63	1.21	1.59	1.18	1.67	1.45	1.71	1.85		1.85
Pt	0.99	1.12	0.74	1.07	0.72	1.15	0.96	1.26	1.6	1.6, 1.7	1.32, 1.315
Rh	2.02	2.14	1.74	2.04	1.66	2.06	1.99	2.24	1.9	2	
Tc	2.83	2.95	2.59	2.90	2.50	2.91	2.84	3.06			

Table 12
Theoretical vacancy formation energies (in eV) predicted by different functionals for bcc metals. The key for $E_f, \widetilde{E}_f$, SH, and PAS are given in Table 11.

El.	LDA		PBE		PW91		PBEsol	revTPSS	Experiment [4,5]	
	E_f	$\widetilde{E}_f$	E_f	$\widetilde{E}_f$	E_f	$\widetilde{E}_f$			SH	PAS
Cr	2.85	2.96	2.77	3.05	2.65	3.01	2.98	3.30	1.2	2.0
Fe	2.30	2.31	2.20	2.22	2.14	2.16	2.47	2.64		
K	0.33	0.35	0.30	0.33	0.29	0.33	0.39	0.38		0.34
Mo	2.87	3.00	2.74	3.07	2.56	3.00	2.90	3.31	1.86, 2.24	3.0, 3.6
Na	0.34	0.51	0.33	0.68	0.31	0.77	0.35	0.33	0.255, 0.35	
Nb	3.01	3.08	2.77	2.95	2.71	2.94	2.99	3.20	1.68, 2.04	2.65
Ta	2.99	3.12	2.82	3.15	2.74	3.18	3.03	3.20		
V			2.27		2.20		2.36	2.59		2.07
W	3.48	3.57	3.31	3.51	3.18	3.45	3.54		3.15, 3.3	4.0, 4.1, 4.6

Table 13
Theoretical vacancy formation energies (in eV) predicted by different functionals for hcp and remaining metals. The key for $E_f, \widetilde{E}_f$, SH, and PAS are given in Table 11.

El.	LDA		PBE		PW91		PBEsol	revTPSS	Experiment [4,5]	
	E_f	$\widetilde{E}_f$	E_f	$\widetilde{E}_f$	E_f	$\widetilde{E}_f$			SH	PAS
Co	2.22	2.32	1.96	2.22	1.90	2.25	2.18	2.48		1.34
Hf	2.17	2.25	2.24	2.42	2.16	2.40	2.32	2.58		
Mg	0.80	0.94	0.77	1.14	0.72	1.21	0.81	0.94		
Os	3.30	3.33	3.03	3.11	2.98	3.09	3.33	3.62	1.8 [59]	
Re	3.65	3.68	3.40	3.48	3.26	3.36	3.68	4.31		
Ru	3.03	3.18	2.71	3.07	2.62	3.08	3.00	3.26		
Sc	1.97	2.10	1.86	2.16	1.80	2.20	1.95	1.98		
Tc	3.05	3.09	2.79	2.88	2.71	2.83	3.05	3.28		
Ti	2.08	2.12	2.08	2.18	1.99	2.13	2.15	2.30	1.55	
Tl	0.53	0.68	0.43	0.81	0.44	0.93	0.52	0.66		0.46
Y	1.91	2.08	1.87	2.29	1.82	2.37	1.95	1.53		
Zn	0.50	0.65	0.42	0.79	0.49	0.97	0.50	0.47	0.61	0.54

0.86 eV, is considered, the difference between revTPSS and experiments is even greater.

The uncertainty surrounding the experimental data on VFEs preclude making definitive conclusions about the accuracy of the different functionals. So, we compared the VFEs predicted by revTPSS and other functionals with the PBE VFE as reference, due to the widespread use of PBE in first principle calculations. The comparison plotted in Fig. 5. shows that LDA consistently over-estimates the VFEs when compared with PBE with a MAPD of 10.4%. VFEs predicted by both the functionals are highly correlated as indicated by the r-value of 0.99. The correlation plot has a slope of 1.03, indicating that the magnitude of difference between LDA and PBE is fairly uniform across all metals. This is in contrast to the trend observed for the cohesive energies. The plot for PW91 in Fig. 5(b) shows that PW91 slightly under-estimates the VFEs when compared with PBE data with a MAPD of 4.2%. Fig. 5(c) shows that PBEsol, similar to LDA, consistently over-estimates the PBE data. The MAPD for PBEsol is closer to that of LDA at 11.1%. The VFEs predicted by the revTPSS functional are higher than the VFEs predicted by all other functionals with the MAPD between revTPSS and PBE VFEs at 20.3%.

The red data points in Fig. 6 show the comparison between the PBEsol VFE data with the VFEs computed by Nazarov et al. using the AM05 functional [23]. Both PBEsol and AM05 functionals

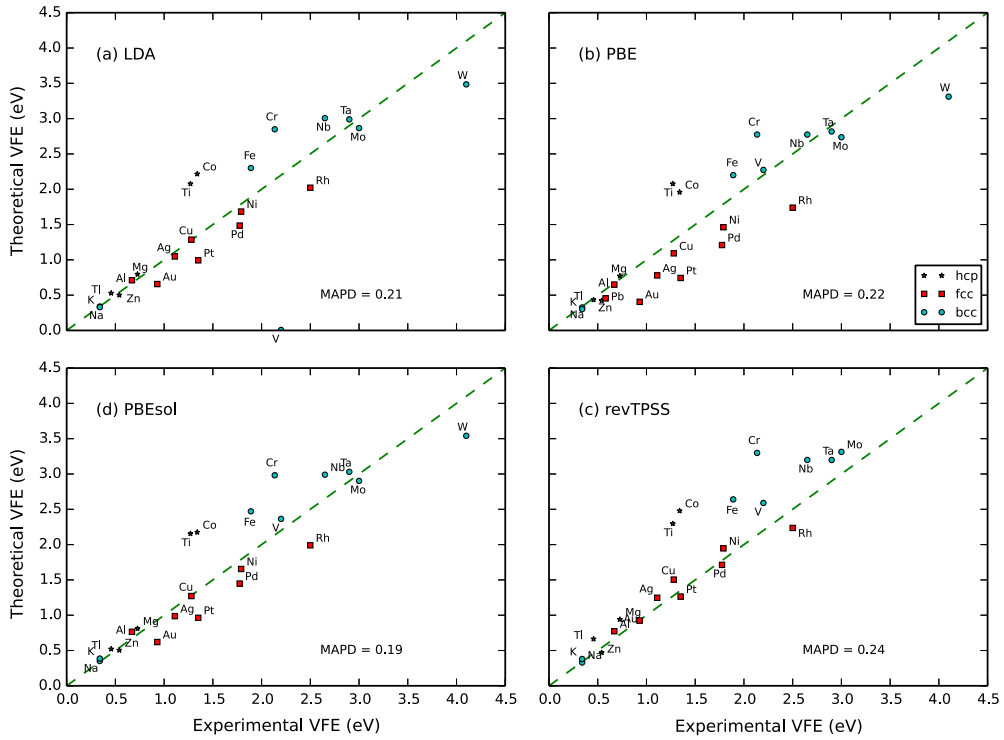

Fig. 3. Comparison between the experimental and the theoretical vacancy formation energies predicted by different functionals. The experimental data is taken from the PAS data compiled in Landolt–Bornstein database for metals [5]. The definition of green dashed line is given in Fig. 1. MAPD stands for "Mean Absolute Percentage Deviation". (For interpretation of the references to color in this figure legend, the reader is referred to the web version of this article.)

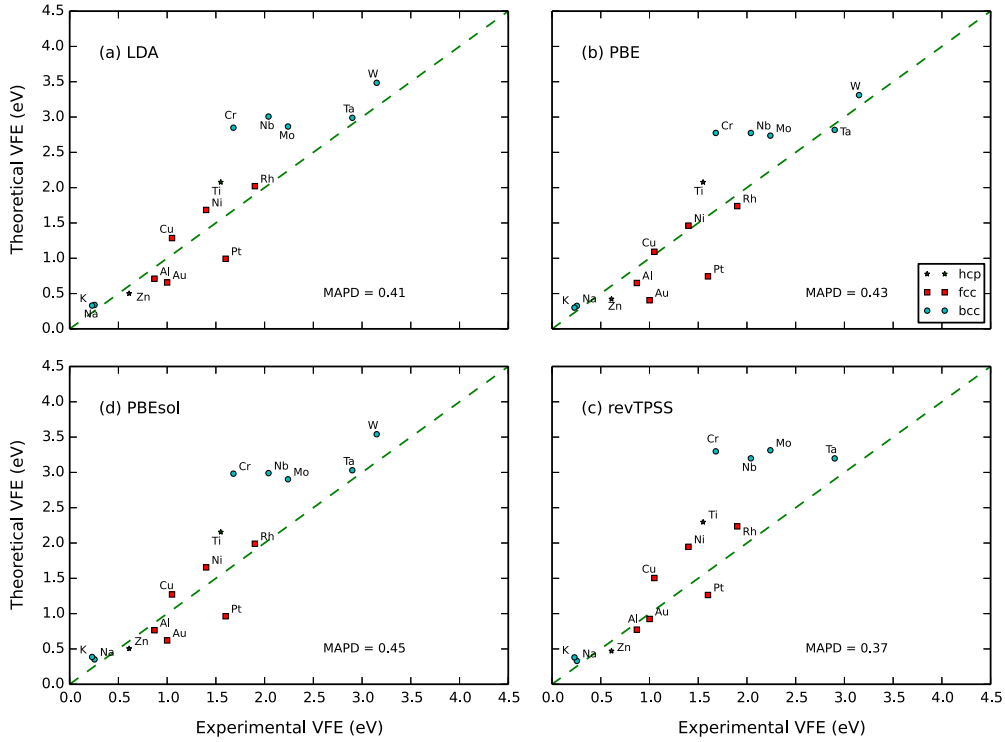

Fig. 4. Comparison between the experimental and the theoretical vacancy formation energies predicted by different functionals. The experimental VFEs are taken from the specific heat data published in Ref. [4] which considers linear temperature dependence for vacancy formation entropy. The definition of green dashed line is given in Fig. 1. MAPD stands for "Mean Absolute Percentage Deviation". (For interpretation of the references to color in this figure legend, the reader is referred to the web version of this article.)

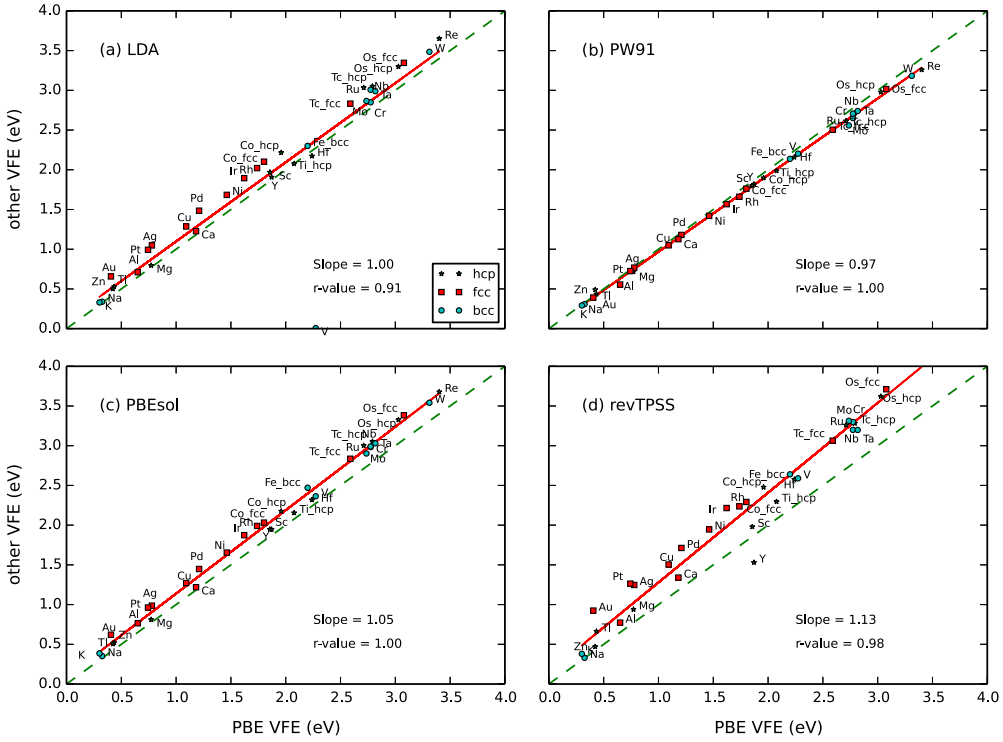

Fig. 5. Comparison between the vacancy formation energies predicted by PBE and other functionals: LDA, PW91, PBEsol, and revTPSS. The definition of red solid and green dashed lines is given in Fig. 1. (For interpretation of the references to color in this figure legend, the reader is referred to the web version of this article.)

predict almost identical VFEs except for a small difference in the case of Au and Ir. This behavior is consistent with their near identical performance in predicting the macroscopic properties. The blue square data points represent the corresponding AM05 VFEs reported in Ref. [16] for Al, Ni and Cu.

Figs. 7–9 show the effect of *a posteriori* surface energy error correction on the computed VFEs. It is clear from the plots in Fig. 7 that the surface energy error correction increases the computed VFEs and brings the VFEs computed with standard LDA and GGA functionals closer. However, the magnitude of the correction is smaller in LDA when compared to GGA functionals. After applying the correction, the MAPD between PBE and LDA VFEs reduces to 2.8% (see Fig. 8) from 10.4%. Fig. 9 shows that for most of the elements, the revTPSS VFEs are higher than the PBE VFEs even after applying the surface energy correction.

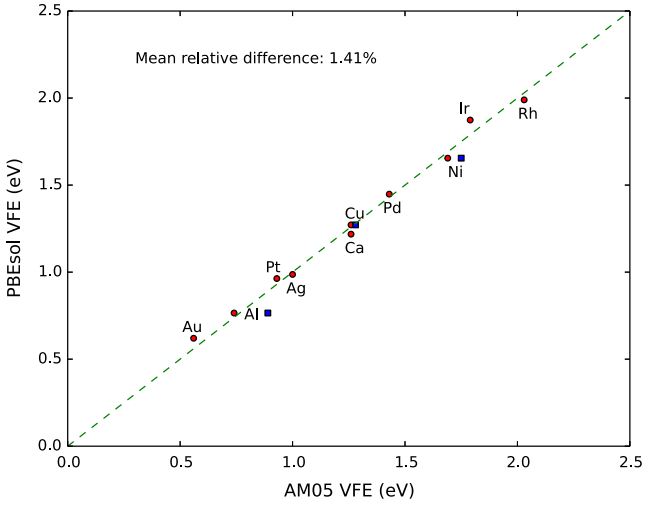

Fig. 6. Comparison between the vacancy formation energies predicted by PBEsol and AM05. The red circle data for AM05 is obtained from Ref. [23], whereas the blue square data for AM05 is obtained from Ref. [16]. The definition of green dashed line is given in Fig. 1. (For interpretation of the references to color in this figure legend, the reader is referred to the web version of this article.)

Of all the functionals studied, revTPSS, a meta-GGA functional, is expected to perform better due to the inclusion of the kinetic energy density term. The contribution from this additional term is responsible for the difference in the VFEs computed with revTPSS and PBE. The MAPD of the VFEs computed with the two functionals is 20.3% indicating that the contribution of the kinetic energy density term to VFEs is significant. Perdew et al. showed that the revTPSS does not have the issue of exchange–correlation surface energy error [34]. But for PBE the surface energy error correction is large. This means the effect of surface energy error is compensated by the contribution coming from the kinetic energy density term. To get the residual contribution of the kinetic energy density term in the VFE predicted by revTPSS, which does not include the effect of surface energy error, we take the difference between revTPSS VFE and the surface energy error corrected PBE VFE. Fig. 9 shows that the residual contribution is mainly positive except for non-transition elements and Zn, Sc and Y. The magnitude of the residual contribution to the revTPSS VFEs is 16.7% of surface energy corrected PBE VFE, when averaged over all the metals.

To understand how vacancy formation energies predicted by revTPSS vary for the metals across the periodic table, VFE is plotted against the Mendeleev Number (MN), a phenomenological number assigned to each element in the periodic table based on its physical, chemical, and electronic characteristics. MN was first proposed by Pettifor for binary compounds [55] and many variants of MN have been proposed in later work. In our work, the MN proposed by Villars et al. [56] is used. Fig. 10 shows the plotted trend, which resembles an inverted parabola. The VFEs reach a maximum for metals whose d-band is half filled. The VFEs that lie in the center

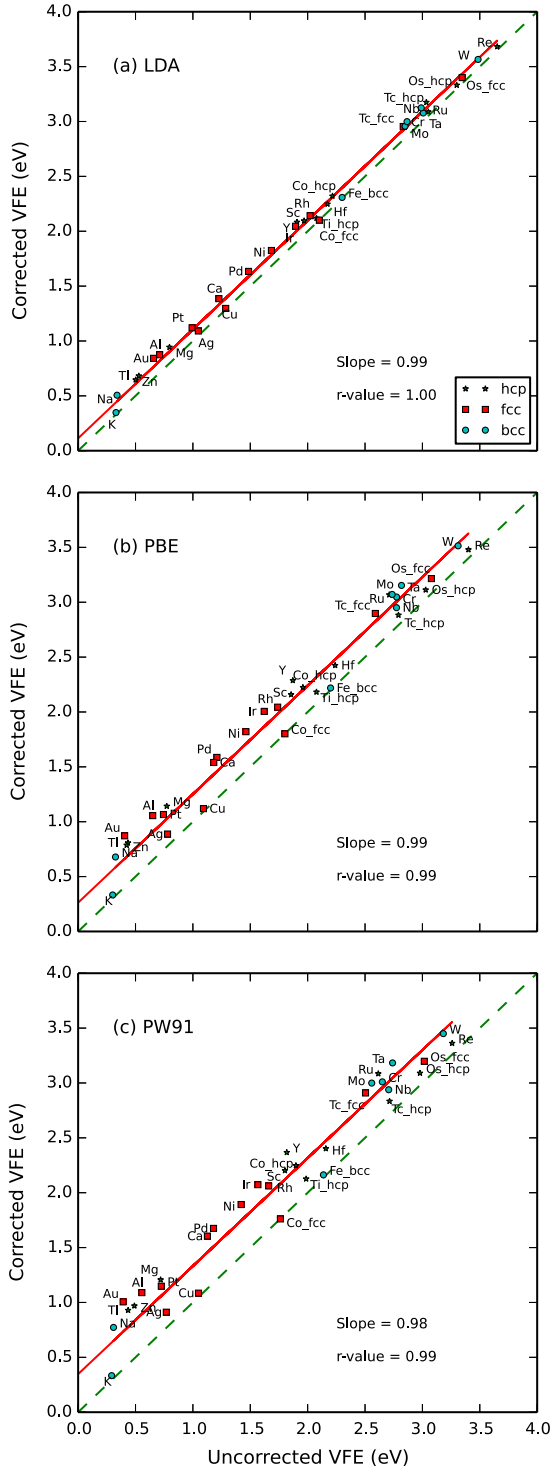

Fig. 7. Vacancy formation energies before and after applying surface error correction. The definition of red solid and green dashed lines is given in Fig. 1. (For interpretation of the references to color in this figure legend, the reader is referred to the web version of this article.)

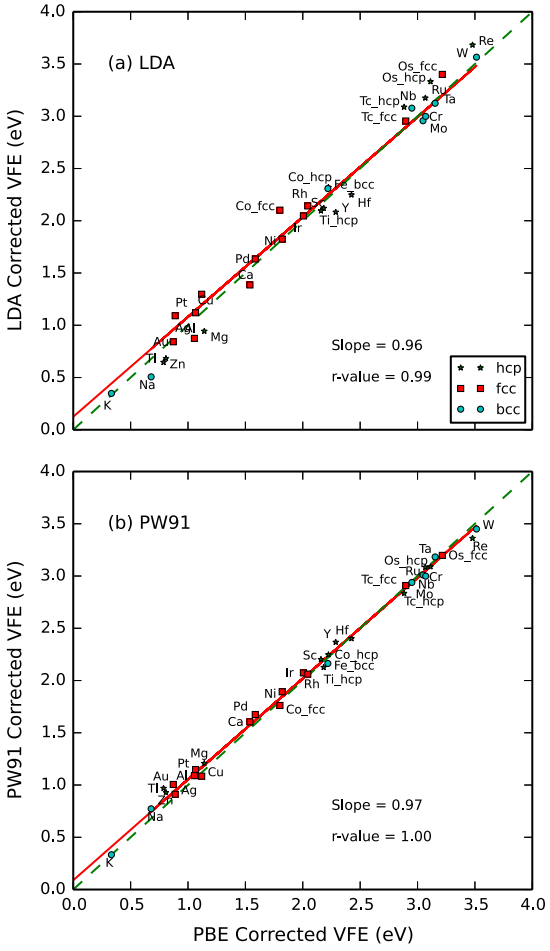

Fig. 8. Comparison between vacancy formation energies predicted by PBE, LDA, and PW91 after applying the surface energy error correction. The definition of red solid and green dashed lines is given in Fig. 1. (For interpretation of the references to color in this figure legend, the reader is referred to the web version of this article.)

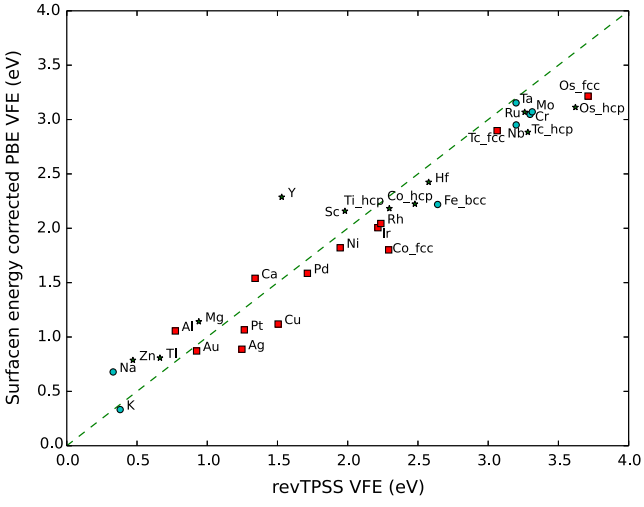

Fig. 9. Comparison between vacancy formation energies predicted by revTPSS functional and surface energy error corrected PBE vacancy formation energies. The definition of green dashed line is given in Fig. 1. (For interpretation of the references to color in this figure legend, the reader is referred to the web version of this article.)

and at the top of the inverted parabola belong to columns 6, 7, and 8 of the periodic table and exhibit a wide variation as we traverse the column. Starting with Co, the VFE values decrease smoothly as the d-bands are filled. Of the elements which exhibit allotropy, for a few elements: Os, Tc, and Co, VFEs for two allotropes are shown.

The parabolic variation of the VFEs across the transition metals described above is similar to the case of the variation of cohesive energy. The relation between VFE and cohesive energy has been empirically suggested to be given as [57]

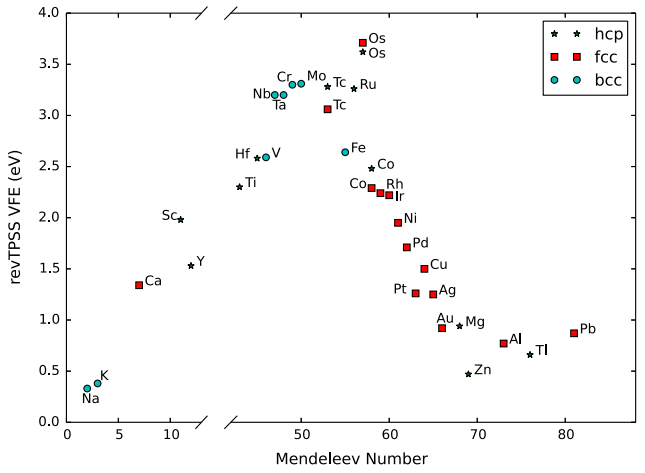

Fig. 10. Vacancy formation energy vs Mendeleev Number for the metallic elements in the periodic table. The vacancy formation energies are computed with revTPSS functional.

$$E_f = \frac{1}{3}E_{coh}. \tag{5}$$

To obtain a corresponding relation between DFT computed VFEs and cohesive energies, correlation between the two quantities is plotted in Fig. 11. The correlation coefficient values of 0.87 and 0.89 indicate that both quantities are not highly correlated. The slope of the green line is 1/3 representing the empirical relation given in Eq. (5). LDA gives a slightly smaller slope of 0.31, whereas PBE and PBEsol give a slightly higher slope of 0.35. The slope of the revTPSS correlation plot is even higher at 0.38. In all the plots, the data points are clustered based on the crystal symmetry indicating that the relation between the cohesive energy and vacancy formation energy is structure dependent. Detailed analysis on the structure dependency of VFEs was reported by Korzavyi et al. previously [15].

4. Summary and conclusions

Vacancy formation energies, lattice constants, cohesive energies and bulk moduli in fcc, bcc and hcp metals have been computed using the revTPSS functional, a self-consistent semilocal meta-generalized gradient approximation functional. The performance of the revTPSS functional has been assessed through comparisons with experimental VFEs, and VFEs computed with four additional density functionals: LDA, PW91, PBE, and PBEsol. The revTPSS functional is found to overestimate the magnitudes of cohesive energies and bulk moduli with a MAPD of 12.08% and 25.47%, respectively, whereas PBE and PW91 show better agreement with the experimental data. We observe that revTPSS in general overestimates the vacancy formation energies when compared to compiled experimental estimates, except for a few metals such Pt, Rh and Zn. However, due to the scatter in the existing experimental data, and the recent report of large anharmonic effects that can sizably affect values extrapolated from high to low temperatures [6], conclusions about the relative accuracy of revTPSS versus LDA and GGA functionals for this quantity are not definitive. The VFEs calculated with revTPSS are significantly larger than those computed by PBE, with a MAPD of 20.3%. Recently, other improved meta-GGA functionals such as MGGA-MS2 [58] have been proposed. A comparison of the meta-GGA functionals with respect to the VFEs would be of interest to better understand the impact of the different kinetic energy density terms in these functionals.

The effect of recently proposed "surface energy correction" schemes on VFEs computed by LDA and GGA functionals have also been assessed. Consistent with results from previous publications [18,19,21,23] these corrections have a larger effect on GGA calculated results compared to LDA. This leads to an improved level of agreement between zero-temperature calculated values and tabu-

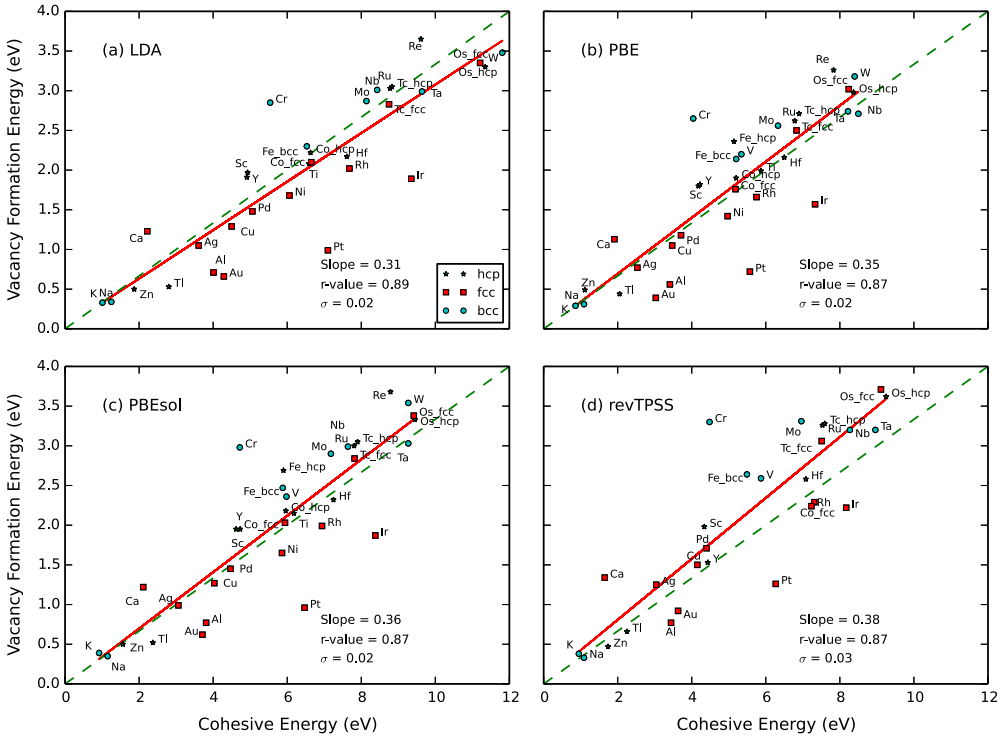

Fig. 11. E_f vs E_{coh} for LDA, PBE, PBEsol and revTPSS functionals. The definitions of red solid and green dashed lines as well as r-value and σ are is given in Fig. 1. (For interpretation of the references to color in this figure legend, the reader is referred to the web version of this article.)

lated experimental values derived from high-temperature measurements [5,4]. However, we note that the recent work of Glensk et al. [6] has shown that, for the case of Cu in particular, commonly-used extrapolations of high-temperature data, which neglect anharmonic vibrational contributions, may lead to sizable errors in derived low-temperature VFEs. These authors show that when such anharmonic corrections are accounted for PBE-GGA gives excellent agreement with both PAS and DD measurements in Al and Cu. As a consequence, further work, which assesses the magnitudes of the anharmonic contributions more generally, is needed to more definitively understand the improvement in accuracy associated with the surface-energy correction schemes. In such studies, the 4d and 5d transition and noble metals, such as Au, Pt, Pd and Rh, would be of particular interest, since these elements show large discrepancies, on the order of 0.53–0.77 eV, with tabulated experimental values.

Acknowledgments

This work at the Lawrence Berkeley National Laboratory was supported by the U.S. Department of Energy under Contract No. DEAC02-05CH11231 under the Materials Project Center grant (award No. EDCBEE). This research used resources of the National Energy Research Scientific Computing Center, which is supported by the Office of Science of the U.S. Department of Energy under Contract No. DEAC02-05CH11231.

References

[1] C. Freysoldt, B. Grabowski, T. Hickel, J. Neugebauer, G. Kresse, A. Janotti, C.G. Van de Walle, Rev. Mod. Phys. 86 (2014) 253, http://dx.doi.org/10.1103/RevModPhys.86.253.
[2] C.G. Van de Walle, J. Neugebauer, J. Appl. Phys. 95 (2004) 3851. http://dx.doi.org/10.1063/1.1682673.
[3] W. Ming, Z. Zak Fang, F. Liu, J. Appl. Phys. 114 (2013) 243502. http://dx.doi.org/10.1063/1.4853055.
[4] Y. Kraftmakher, Equilibrium Vacancies and Thermophysical Properties of Metals, Physics reports, North-Holland, Elsevier, 1998.
[5] P. Ehrhart, P. Jung, H. Schultz, H. Ullmaier, Atomic Defects in Metals, Zahlenwerte und Funktionen aus Naturwissenschaften und Technik: Kristall- und Festkörperphysik, vol. 25, Springer-Verlag, Berlin, 1991.
[6] A. Glensk, B. Grabowski, T. Hickel, J. Neugebauer, Phys. Rev. X 4 (2014) 011018.
[7] W. Kohn, L. Sham, Phys. Rev. 140 (1965) 1133.
[8] R.M. Dreizler, E.K.U. Gross, Density Functional Theory, Springer, Berlin, 1990.
[9] J.P. Perdew, S. Kurth, in: C. Fiolhais, F. Nogueira, M. Marques (Eds.), A Primer in Density Functional Theory, Springer, Berlin, 1990.
[10] P. Perdew, K. Burke, M. Ernzerhof, Phys. Rev. Lett. 77 (1996) 3865.
[11] J.P. Perdew, Y. Wang, Phys. Rev. B 45 (1992) 13244.
[12] J.P. Perdew, J.A. Chevary, S.H. Vosko, K.A. Jackson, M.R. Pederson, D.J. Singh, C. Fiolhais, Phys. Rev. B 46 (1992) 6671.
[13] J.P. Perdew, Y. Wang, Phys. Rev. B 45 (1992) 13244.
[14] N. Chetty, M. Weinert, T.S. Rahman, J.W. Davenport, Phys. Rev. B 52 (1995) 6313.
[15] P.A. Korzhavyi, I.A. Abrikosov, B. Johansson, A.V. Ruban, H.L. Skriver, Phys. Rev. B 59 (1999) 11693.
[16] L. Delczeg, E.K. Delczeg-Czirjak, B. Johansson, L. Vitos, J. Phys.: Cond. Matter 23 (2011) 045006.
[17] L. Delczeg, E.K. Delczeg-Czirjak, B. Johansson, L. Vitos, Phys. Rev. B 80 (2009) 205121.
[18] K. Carling, G. Wahnström, T.R. Mattsson, A.E. Mattsson, N. Sandberg, G. Grimvall, Phys. Rev. Lett. 85 (2000) 3862.
[19] T.R. Mattsson, A.E. Mattsson, Phys. Rev. B 66 (2002) 214110.
[20] K.M. Carling, G. Wahnström, T.R. Mattsson, N. Sandberg, G. Grimvall, Phys. Rev. B 67 (2003) 054101.
[21] P.K. Nandi, M.C. Valsakumar, S. Chandra, H.K. Sahu, C.S. Sundar, J. Phys.: Condens. Matter 22 (2010) 345501.
[22] R.Q. Hood, P.R.C. Kent, F.A. Reboredo, Phys. Rev. B 85 (2012) 134109.
[23] R. Nazarov, T. Hickel, J. Neugebauer, Phys. Rev. B 85 (2012) 144118.
[24] T. Angsten, T. Mayeshiba, H. Wu, D. Morgan, New J. Phys. 16 (2014) 015018.
[25] A.E. Mattsson, W. Kohn, J. Chem. Phys. 115 (2001) 3441.
[26] A. Michaelides, M. Scheffler, An introduction to the theory of crystalline elemental solids and their surfaces, in: K. Wandelt (Ed.), Surface and Interface Science, vol. 1, Wiley, 2012.
[27] J.L.D. Silva, C. Stampfl, M. Scheffler, Surf. Sci. 600 (2006) 703.
[28] R. Armiento, A.E. Mattsson, Phys. Rev. B 72 (2005) 085108.
[29] A.E. Mattsson, R.R. Wixom, R. Armiento, Phys. Rev. B 77 (2008) 155211.
[30] J.P. Perdew, A. Ruzsinszky, G.I. Csonka, O.A. Vydrov, G.E. Scuseria, L.A. Constantin, X. Zhou, K. Burke, Phys. Rev. Lett. 100 (2008) 136406.
[31] L. Vitos, B. Johansson, J. Kollár, H.L. Skriver, Phys. Rev. B 62 (2000) 10046.
[32] A.E. Mattsson, R. Armiento, T.R. Mattsson, Phys. Rev. Lett. 101 (2008) 239701.
[33] Y. Zhao, D.G. Truhlar, J. Chem. Phys. 125 (19) (2006) 194101.
[34] J.P. Perdew, A. Ruzsinszky, G.I. Csonka, L.A. Constantin, J. Sun, Phys. Rev. Lett. 103 (2009) 026403.
[35] J.P. Perdew, A. Ruzsinszky, G.I. Csonka, L.A. Constantin, J. Sun, Phys. Rev. Lett. 106 (2011) 179902(E).
[36] J. Sun, B. Xiao, Y. Fang, R. Haunschild, P. Hao, A. Ruzsinszky, G.I. Csonka, G.E. Scuseria, J.P. Perdew, Phys. Rev. Lett. 111 (2013) 106401.
[37] J. Tao, J.P. Perdew, V.N. Staroverov, G.E. Scuseria, Phys. Rev. Lett. 91 (2003) 146401.
[38] J. Sun, M. Marsman, G.I. Csonka, A. Ruzsinszky, P. Hao, Y. Kim, G. Kresse, J.P. Perdew, Phys. Rev. B 84 (2011) 035117.
[39] G. Kresse, J. Hafner, Phys. Rev. B 47 (1993) 558.
[40] G. Kresse, J. Hafner, Phys. Rev. B 49 (1994) 14251.
[41] G. Kresse, J. Furthmuller, Phys. Rev. B 54 (1996) 11169.
[42] A. Jain, S.P. Ong, G. Hautier, W. Chen, W.D. Richards, S. Dacek, S. Cholia, D. Gunter, D. Skinner, G. Ceder, K.a. Persson, APL Mater. 1 (1) (2013) 011002, http://dx.doi.org/10.1063/1.4812323.
[43] S.P. Ong, W.D. Richards, A. Jain, G. Hautier, M. Kocher, S. Cholia, D. Gunter, V.L. Chevrier, K.A. Persson, G. Ceder, Comput. Mater. Sci. 68 (2013) 314.
[44] P.E. Blöchl, Phys. Rev. B 50 (1994) 17953.
[45] G. Kresse, J. Joubert, Phys. Rev. B 59 (1999) 1758.
[46] M. Methfessel, A.T. Paxton, Phys. Rev. B 40 (1989) 3616.
[47] R. Soulairol, C.-C. Fu, C. Barreteau, Phys. Rev. B 83 (2011) 214103.
[48] A.E. Mattsson, R. Armiento, P.A. Schultz, T.R. Mattsson, Phys. Rev. B 73 (2006) 195123.
[49] F. Birch, Phys. Rev. 71 (1947) 809.
[50] N.W. Ashcroft, M.N.D., International Union of Crystallography, Chester, England, 1987.
[51] Y. Wang, S. Curtarolo, C. Jiang, R. Arroyave, T. Wang, G. Ceder, L.-Q. Chen, Z.-K. Liu, Calphad 28 (2004) 79.
[52] C. Kittel, Introduction to Solid State Physics, eighth ed., John Wiley & Sons, Inc., Hoboken, NJ, 2005.
[53] A. James, M. Lord, Macmillan's Chemical and Physical Data, Macmillan, London, UK, 1992.
[54] G. Kaye, T. Laby, Tables of Physical and Chemical Constants, 15th ed., Longman, London, UK, 1993.
[55] D.G. Pettifor, Solid State Commun. 51 (1981) 31.
[56] P. Villars, K. Cenzual, J. Daams, Y. Chen, I.S., J. Alloys Compd. 367 (2004) 167.
[57] T. Górecki, Z. Metallkd. 65 (1974) 426.
[58] J. Sun, B. Xiao, Y. Fang, R. Haunschild, P. Hao, A. Ruzsinszky, G.I. Csonka, G.E. Scuseria, J.P. Perdew, Phys. Rev. Lett. 111 (2013) 106401.
[59] V. Chekhovskoi, V. Tarasov, High Temp. 50 (2012) 722.